# Homoclinic Snaking of Localized Patterns in a Spatially Forced System

F. Haudin,[1] R. G. Rojas,[2] U. Bortolozzo,[1] S. Residori,[1] and M. G. Clerc[3]

[1]*INLN, Université de Nice-Sophia Antipolis, CNRS, 1361 route des Lucioles 06560 Valbonne, France*
[2]*Instituto de Física, Pontificia Universidad Católica de Valparaíso, Casilla 4059, Valparaíso, Chile*
[3]*Departamento de Física, FCFM, Universidad de Chile, Casilla 487-3, Santiago Chile*

(Received 29 July 2011; published 22 December 2011)

Dissipative localized structures exhibit intricate bifurcation diagrams. An adequate theory has been developed in one space dimension; however, discrepancies arise with the experiments. Based on an optical feedback with spatially modulated input beam, we set up a 1D forced configuration in a nematic liquid crystal layer. We characterize experimentally and theoretically the homoclinic snaking diagram of localized patterns, providing a reconciliation between theory and experiments.

DOI: 10.1103/PhysRevLett.107.264101 PACS numbers: 05.45.−a, 02.30.Oz, 42.65.−k, 45.70.Qj

Localized patterns arise in dissipative and spatially extended systems and can be seen as the single or multicells units into which it is possible, under certain circumstances, to decompose a pattern. Characterized by a family of continuous parameters, as position, amplitude and width, localized patterns can, formally, be described as particle-like objects, even though made of a large number of fundamental constituents—atoms or molecules. Their universal nature leads to observe them in such different fields as magnetic materials, liquid crystals, gas discharge systems, chemical reactions, fluids, granular media, nonlinear optics, and Bose-Einstein condensates [1–3]. Many experimental and theoretical works have been devoted to the study of localized patterns, and different mechanisms have been identified as being responsible for their appearance. Additionally, intriguing dynamical behaviors, displaying mutual interaction of localized structures, have been reported and control methods have been developed in view of potential applications, these mainly aimed at using single-cell localized structures as elementary, erasable and rewritable, storage bits.

A soliton is an example of a macroscopic localized object, which arises from the balance between dispersion and nonlinearity. Solitons have been reported in various fields such as fluid dynamics, nonlinear optics, and Hamiltonian systems [4]. Localized patterns can be considered as a generalization of this concept to out of equilibrium, dissipative systems. Usually emerging in the region of bistability between a uniform and a pattern state, localized patterns extend over a limited space region and consist of only a few cells, eventually a single one, of the corresponding extended structure. While a front connecting two uniform states has to be motionless only in a specific point of the parameter space, the so-called the Maxwell point [5], when one of the two states is a pattern the corresponding orbits in the phase space of the equivalent dynamical system exhibit heteroclinic tangle, leading to a family of localized solutions with increasing number of spatial oscillations. This description corresponds to the well-known homoclinic snaking bifurcation [6], which occurs in the pinning range of the front solution [7,8]. The scenario has been studied numerically in various physical contexts [1,3]; however, an experimental validation has been proposed only for vertical-cavity semiconductor lasers [9] and gas discharge systems [2]. In general, several discrepancies arise when comparing the experimental observations with theory. For instance, the extent of the bistability region is not always consistent with that expected from theory. Other discrepancies come from the difficulty to unambiguously distinguish between a bound state of localized structures and a multicells localized pattern. For example, in a liquid crystal light-valve experiment, bifurcation diagrams of localized patterns with different symmetries have been reported [10,11], thus showing that coexistence of localized patterns can be due to mechanisms other than the heteroclinic tangle. Hence, the conclusions drawn when comparing theory and experiments are not decisive.

In this Letter, we propose a new strategy to elucidate the mechanism of homoclinic snaking of localized patterns. Our approach is based on introducing a spatial forcing in a system that exhibits bistability between two uniform states. Because of the spatial forcing, the uniform states become periodic (patterns) and the stationary behavior of the dynamical system becomes equivalent to that previously described: the orbits in the stationary phase space show heteroclinic tangle, leading to a family of localized solutions with increasing number of spatial oscillations. When referring to the equivalent temporal system, a straightforward analogy can be drawn by considering, for instance, the effect of a forcing on the orbits of an oscillator [12]. Recently, by using a similar strategy, we have shown that it is possible to characterize the pinning range and the bistability region of patterns [13], confirming that localized patterns may appear as a consequence of front interaction [14]. More precisely, here we consider a setup based on a nematic liquid crystal layer and a 1D spatially modulated optical feedback. In a large region of the parameter space

 

the system exhibits bistability between two different average orientations of the liquid crystal molecules. Because of the spatial forcing, a large and controlled pinning range exists, within which a family of localized patterns can be carefully addressed, thus allowing us to construct a detailed snaking bifurcation diagram, which is consistent with the theory.

*Experimental setup and results.*—The experiment consists of a liquid crystal light valve (LCLV) with optical feedback. The LCLV is made of a thin nematic liquid crystal (LC) layer inserted in between a glass plate and a photoconductive wall over which a dielectric mirror is deposited. An externally applied $V_0$ voltage induces an electric field, in the direction of which molecules tend to orientate. When reflected by the mirror, and after passing through the LC layer, light acquires a phase shift that is a function of the LC orientation angle, which depends on the light intensity $I_w$ present on the photoconductive side of the LCLV [15]. A spatial light modulator (SLM) controls the light intensity profile at the entrance of the feedback loop, which is closed by a fiber bundle. The intensity distribution at the SLM is exactly imaged on the LCLV and the rear side of the fiber bundle. In this configuration the system exhibits bistability between uniform states [15]. We use $V_0$ as a control parameter, whereas the other parameters are similar to those considered in [13]. By using the SLM, suitable intensity masks are produced in order to impose a quasiunidimensional spatially periodic forcing, which is responsible for the uniform states to become spatially periodic ones. Hence, the system presents coexistence of patterns and we expect to observe localized patterns [16,17].

We first characterize the pinning region, then, by using the SLM, we selectively create localized patterns with a different number of elementary cells. A single-cell and a two-cells structure are reported in Figs. 1(a) and 1(b), respectively. It is worth noting that a two-cells structure is different from a bound state of two single-cell structures. In our system, this distinction becomes clear and can be verified by the selective writing and erasure of single cells, as allowed by the spatial forcing method. This is a major difference with respect to previous experiments, where localized patterns arise spontaneously and are difficult to control [18], unless pinned over an underlying grid potential [19]. Moreover, in the present case the bistability is between two patterns: a small amplitude spatially modulated lower state and a larger amplitude spatially modulated upper state.

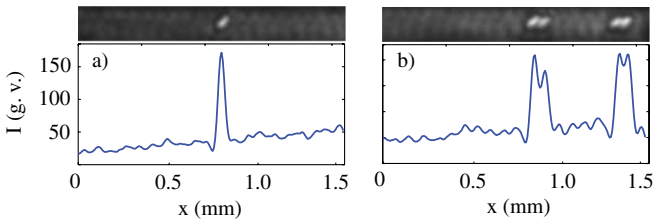


FIG. 1 (color online). Snapshots (top) and corresponding 1D intensity profiles (bottom) of experimental localized patterns: (a) an isolated one-cell pattern, (b) a bound state of two-cells patterns. g.v. represents gray values.

By varying the external voltage $V_0$, we characterize the region of coexistence of different localized patterns and we construct the homoclinic snaking bifurcation diagram. With this purpose, we measure the total intensity. This quantity is proportional to the area of the pattern, each localized pattern being characterized by a different number of cells, and is consistent with the numerical representations, usually measuring the area of the patterns [6]. Figure 2 shows the results. Examples of the typical localized patterns observed in the coexistence region are schematically reported in Fig. 2(a), where the intensity profile is shown together with the corresponding experimental snapshot for $n$-cells localized patterns, with $n$ from 1 to 9. The low amplitude pattern and the large amplitude pattern are also shown, respectively, at the bottom and at the top of the figure. The total extension of the system is of approximately 12 cells. Larger patterns are difficult to obtain because of spatial inhomogeneities in the system.

Figure 2(b) displays the snaking bifurcation diagram as a function of the applied voltage $V_0$. The different lines inside the coexistence region (light shadow) mark stable localized structures with a different number of cells. By decreasing $V_0$, we observe that localized patterns shrink and become smaller until they reach the lowest state, that is, the small amplitude pattern. On the other side, by increasing $V_0$, localized patterns expand, developing an increasing number of spatial oscillations until they reach the uppermost state, that is, the large amplitude pattern. Within the experimental accuracy, and up to the structure with $n = 6$, the oscillations of the snaking diagram are consistent with previously derived analytical results [14,20]. However, when going towards the top of the diagram the branches become slanted. As we will see in the following, this effect can be explained by considering the influence of spatial inhomogeneities in the system.

*Theoretical description.*—The dynamics of the system is characterized by the reorientation of the LC molecules, which is phenomenologically described by a relaxation equation for the average tilt angle $\theta(x, t)$, $0 \leq \theta \leq \pi/2$, and is driven by the feedback light intensity $I_w$ [15,18]. Thus, the model reads as

$$\tau_{\mathrm{LC}} \partial_t \theta = l^2 \partial_{xx} \theta - \theta + \frac{\pi}{2}\left(1 - \sqrt{\frac{V_{\mathrm{FT}}}{\Gamma V_0 + \alpha I_w(\theta)}}\right), \quad (1)$$

where $x$ is the transverse direction of the LC layer, $\tau_{\mathrm{LC}}$ the LC relaxation time, $l$ the electrical coherence length, and $\Gamma V_0 + \alpha I_w \geq V_{\mathrm{FT}}$ the effective voltage applied to the LC layer, with $V_{\mathrm{FT}}$ the threshold for the Fréedericksz transition, $\Gamma$ the overall impedance of the LCLV dielectric

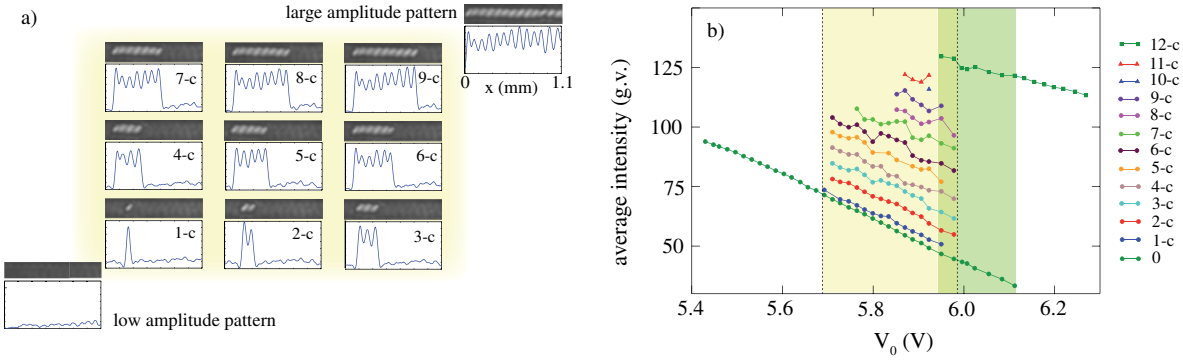


FIG. 2 (color online). Homoclinic snaking bifurcation of localized patterns. (a) Snapshot (top) and corresponding 1D intensity profile (bottom) of the typically observed patterns; the number of cells increases from bottom to top. (b) Total intensity as a function of the external voltage $V_0$, showing the homoclinc snaking diagram of localized patterns; $n$-c stands for $n$-cell localized structure. The light shadow area marks the region of coexistence of localized patterns, while the dark shadow area denotes the region of bistability between the two extended patterns.

layers, and $\alpha$ a phenomenological parameter summarizing, in the linear approximation, the response of the photoconductor [15]. In the presence of the spatial forcing the light intensity reaching the photoconductor is

$$I_w(\theta) = I_{\text{in}}\left[1 + B\sin\left(\frac{2\pi x}{p}\right)\right][1 + \cos(\beta\cos^2\theta)], \quad (2)$$

where $I_{\text{in}}$ is the total input intensity, $B$ and $p$ are, respectively, the amplitude and period of the forcing, and $\beta\cos^2\theta$ the overall phase shift experienced by the light traversing the LC layer. Here, $\beta = 2kd\Delta n$, with $d$ the thickness of the nematic layer, $\Delta n$ the LC birefringence, and $k = 2\pi/\lambda$ with $\lambda$ the laser wavelength.

The model Eqs. (1) and (2) present coexistence between patterns [13]. These are characterized by different amplitudes due to the fact that the forcing is composed of an additive and a multiplicative part (the feedback intensity depends on $\theta$). Figure 3 illustrates the typical extended and localized patterns obtained with this model. In

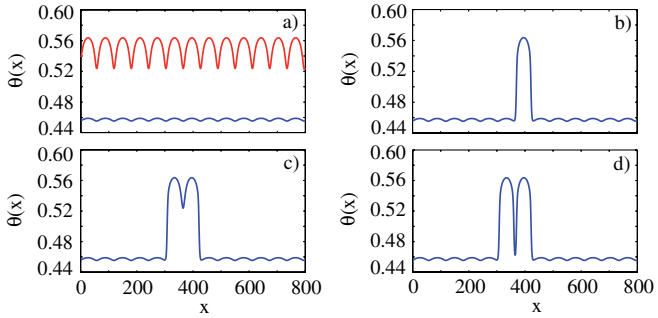


FIG. 3 (color online). Steady states obtained from model Eqs. (1) and (2), $V_{\text{FT}} = 3.2$ V, $V_0 = 6.3$ V, $I_{\text{in}} = 1.2\,\text{mW/cm}^2$, $\Gamma = 1$, $\beta = 59$, $B = 0.77$, $p = 0.077$: (a) coexistence of patterns, (b) localized one-cell pattern, (c) localized two-cells pattern, and (d) bound state of two localized structures of one cell.

Fig. 3(a) we can appreciate the difference of oscillation amplitude for the lowest and uppermost pattern, whereas in Fig. 3(b) a single-cell localized structure is shown. Figures 3(c) and 3(d) emphasize the different nature of the solution with two-cells and the bound state of two localized structures, respectively. In one spatial dimension, theoretically and numerically, it is simple to distinguish between these solutions that correspond, respectively, to a single homoclinic and a double homoclinic orbit. Nevertheless, to distinguish them experimentally is a complex task, which becomes more and more complex as one considers all the possible combinations of cells. A mixture of these solutions in the bifurcation diagram generates enormous distortions of the snaking sequence, which was predicted only for multiple-cell patterns and in one dimension. In our experiment we achieve a high degree of control of localized states and the system is constrained to be quasi-one-dimensional. However, the case with two single-cells localized structures is quite delicate to stabilize unless an empty cell is left between the two.

Numerically, we have measured the total intensity $I_{\text{total}} = \int_0^L dx I_w[\theta(x)]$, where $L$ is the size of the system, and we have constructed the bifurcation diagram of localized patterns as a function of the control parameter $V_0$, as displayed in Fig. 4(a). This snaking diagram gives results very similar to those observed in simple unforced models like the Swift-Hohenberg equation [21]. The most significative difference is that, when increasing the amplitude of the forcing, the bistability region between the two patterns shrinks. This causes the snaking bifurcation diagram to shift outside the bistable region [see Fig. 4(a)], with the coexistence region of localized patterns occurring in a different range of parameters. This behavior is consistent with the experimental findings [see Fig. 2(b)].

Moreover, the snaking region is contained in a slightly slanted rectangular area, consistent with the first 6 experimental branches of localized patterns. However, the last 5

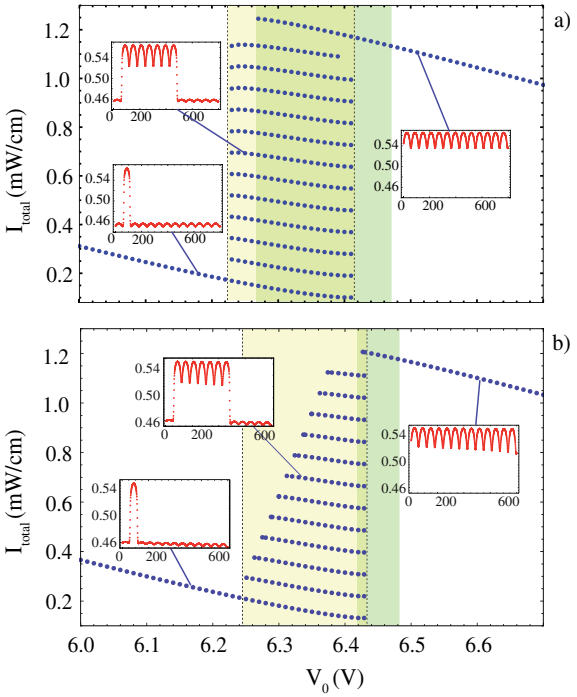


FIG. 4 (color online). Homoclinic snaking diagrams from model Eqs. (1) and (2), same parameters as for Fig. 3: (a) homogeneous voltage, (b) inhomogeneous voltage, $\delta V/L = 0.025$; the inset images are the corresponding localized patterns.

experimental branches are more slanted. To account for these observations, we include in the model a spatial inhomogeneity of the parameters. For instance, we consider a small gradient of the voltage, $V_0(x) = V_0 + x\delta V/L$, in order to reproduce the weak intensity gradient visible in the experimental patterns (see Fig. 1). The resulting bifurcation diagram, and associated patterns, are displayed in Fig. 4(b). Because of the spatial inhomogeneity, the snaking diagram becomes tilted, with each successive saddle-node bifurcation now occurring at an increasingly larger voltage from bottom to top. Additionally, the bistability region is highly reduced and the uppermost pattern is located at the edge of the snaking region, similarly to what is observed experimentally.

Finally, we have considered the influence of the forcing amplitude on the extent of the snaking region. The numerical results are reported in Fig. 5, where the region of coexistence of localized patterns is plotted in the $V_0 - B$ parameter space. For low forcing amplitude the size of the snaking region increases with $B$; however, it decreases at large forcing amplitude because of the saddle-node bifurcation occurring when the uppermost state reaches the lowest one [16]. As for the influence of the forcing wavelength $p$, its variation only introduces a rescaling of the pattern wavelength [13].

*Conclusions.*—One-dimensional spatially forced systems allow us to characterize the complex organization of localized patterns in the homoclinic snaking diagram.

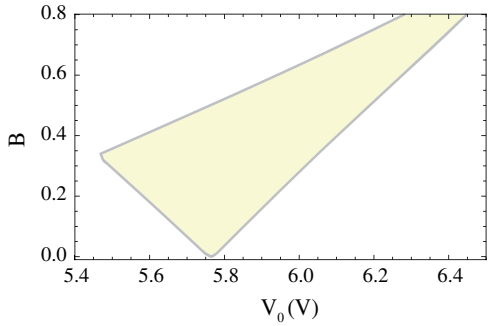


FIG. 5 (color online). Snaking region (shaded area), corresponding to the coexistence region of localized patterns, in the $V_0 - B$ parameter space.

Our experimental observations are consistent with the theoretical results. However, it is important to remark that the snaking diagram is structurally fragile, since small effects generate large deformations, which explains the difficulty of achieving experimental verification.

We acknowledge financial support of the ANR international program, project ANR-2010-INTB-402-02 (ANR-CONICYT39), "COLORS." M. G. C. and R. G. R. acknowledge financial support of the FONDECYT project 1090045, 11080286, and ACT project 127.

[1] O. Descalzi, M. Clerc, S. Residori, and G. Assanto, *Localized States in Physics: Solitons and Patterns* (Springer, New York, 2011).
[2] H. G. Purwins, H. U. Bodeker, and Sh. Amiranashvili, Adv. Phys. **59**, 485 (2010).
[3] T. Ackemann, W. J. Firth, and G. L. Oppo, Adv. At. Mol. Opt. Phys. **57**, 323 (2009).
[4] A. C. Newell, *Solitons in Mathematics and Physics* (Society for Industrial and Applied Mathematics, Philadelphia, 1985).
[5] R. Goldstein *et al.*, Phys. Rev. A **43**, 6700 (1991).
[6] P. D. Woods and A. R. Champneys, Physica (Amsterdam) **129D**, 147 (1999).
[7] Y. Pomeau, Physica (Amsterdam) **23D**, 3 (1986).
[8] P. Coullet, C. Riera, and C. Tresser, Phys. Rev. Lett. **84**, 3069 (2000).
[9] S. Barbay *et al.*, Phys. Rev. Lett. **101**, 253902 (2008).
[10] U. Bortolozzo *et al.*, Phys. Rev. Lett. **93**, 253901 (2004).
[11] M. Ayoub *et al.*, Eur. Phys. J. D **59**, 133 (2010).
[12] S. Wiggins, *Introduction to Applied Nonlinear Dynamical Systems and Chaos* (Springer-Verlag, New York, 1990).
[13] F. Haudin *et al.*, Phys. Rev. Lett. **103**, 128003 (2009); Phys. Rev. E **81**, 056203 (2010).
[14] M. G. Clerc and C. Falcon, Physica (Amsterdam) **356A**, 48 (2005).
[15] S. Residori, Phys. Rep. **416**, 201 (2005).
[16] U. Bortolozzo *et al.*, Phys. Rev. Lett. **96**, 214501 (2006), New J. Phys. **11**, 093037 (2009).

[17] U. Bortolozzo *et al.*, Int. J. Opt. (**2009**) 926810; M. G. Clerc *et al.*, Eur. Phys. J. D **59**, 43 (2010).
[18] M. G. Clerc, A. Petrossian, and S. Residori, Phys. Rev. E **71**, 015205(R) (2005).
[19] U. Bortolozzo and S. Residori, Phys. Rev. Lett. **96**, 037801 (2006).
[20] G. Kozyreff and S. J. Chapman, Phys. Rev. Lett. **97**, 044502 (2006).
[21] S. M. Houghton and E. Knobloch, Phys. Rev. E **80**, 026210 (2009).